Pressure-induced polar phases in relaxor multiferroic $PbFe_{0.5}Nb_{0.5}O_3$

D. P. Kozlenko,[1] S. E. Kichanov,[1] E. V. Lukin,[1] N. T. Dang,[2] L. S. Dubrovinsky,[3] H.-P. Liermann,[4] W. Morgenroth,[5] A. A. Kamynin,[6] S. A. Gridnev,[6] and B. N. Savenko[1]

[1]*Frank Laboratory of Neutron Physics, Joint Institute for Nuclear Research, 141980 Dubna, Russia*
[2]*Center of Research and Development, Duy Tan University, 550000 Da Nang, Vietnam*
[3]*Bayerisches Geoinstitut, University Bayreuth, D-95440 Bayreuth, Germany*
[4]*Photon Sciences, Deutsches Elektronen Synchrotron, D-22607 Hamburg, Germany*
[5]*Institute of Geosciences, University of Frankfurt, D-60438 Frankfurt, Germany*
[6]*Voronezh State Technical University, Moskovskii pr, 14, 394026 Voronezh, Russia*

(Received 23 January 2014; revised manuscript received 31 March 2014; published 16 May 2014)

The structural, magnetic, and vibrational properties of $PbFe_{0.5}Nb_{0.5}O_3$ relaxor multiferroic have been studied by means of x-ray, neutron powder diffraction, and Raman spectroscopy at pressures up to 30 GPa. Two successive structural phase transitions from the initial $R3m$ polar phase to Cm and Pm monoclinic polar phases were observed at $P = 5.5$ and 8.5 GPa. Both transitions are associated with anomalies in pressure behavior of several stretching and bending modes of oxygen octahedra as well as Fe/Nb localized vibrational modes. The G-type antiferromagnetic order remains stable upon compression up to 6.4 GPa, assuming possible multiferroic properties of pressure-induced phases. The Néel temperature increases with a pressure coefficient $(1/T_N)dT_N/dP = 0.012$ GPa^{-1}. The observed pressure-induced phenomena in $PbFe_{0.5}Nb_{0.5}O_3$ are in drastic contrast with conventional multiferroics, exhibiting a general tendency towards a suppression of polar phases and/or magnetoelectric coupling under pressure.

DOI: 10.1103/PhysRevB.89.174107 PACS number(s): 61.50.Ks, 75.25.−j, 78.30.−j

I. INTRODUCTION

The multiferroic materials, revealing a coupling between ferroelectric and magnetic orders, recently have become the focus of extensive scientific research. A coexistence of ferroelectric polarization and magnetic order in such materials provides a route for a construction of novel electronic devices with a possibility to control magnetic properties by electric field and vice versa [1–3].

The two types of multiferroic materials are generally known. In the first one, classical multiferroics, such as $BiFeO_3$ and hexagonal $RMnO_3$ (R = Ho, Y, Lu, . . .), the ferroelectricity and magnetism have different origins and coupled relatively weakly, leading to substantially larger ferroelectric transition temperatures with respect to magnetic ordering ones [1,2]. In the second one, discovered quite recently, the ferroelectricity appears due to violation of the inversion symmetry of the crystal structure by incommensurate magnetic order. Typical representatives of these materials are orthorhombic $RMnO_3$, RMn_2O_5 (R = rare earth elements), and $RbFe(MoO_4)_2$, which exhibit strong magnetoelectric coupling, close ferroelectric transition, and magnetic ordering temperatures [3–5].

An unusual type of multiferroic material, with properties distinctive from those described above, is the lead ferroniobate $PbFe_{0.5}Nb_{0.5}O_3$, exhibiting a pronounced magnetoelectric coupling [1,6]. In addition, lead ferroniobate is a promising basic compound for a development of piezoelectric, electrostrictive, capacitor, and pyroelectric materials [1,7,8]. Due to a chemical disorder of magnetic Fe^{3+} and nonmagnetic Nb^{5+} ions, having different charges and randomly occupying the same crystallographic sites, $PbFe_{0.5}Nb_{0.5}O_3$ demonstrates a relaxor ferroelectric behavior and a coexistence of the spin-glass and long-range magnetic order [9–11]. In the paraelectric phase, $PbFe_{0.5}Nb_{0.5}O_3$ has an ideal perovskite cubic structure of $Pm\bar{3}m$ symmetry [12]. Below the ferroelectric transition temperature, $T_C = 376$ K, the tetragonally distorted structure of $P4mm$ symmetry is formed [13]. Below $T_t = 355$ K, another polar phase is formed. Its symmetry is still debated, and two structural models were proposed: a rhombohedral $R3m$ one [12,14], supported by the analysis of the experimental behavior of the quadratic paramagnetoelectric effect [10], and an alternative monoclinic Cm one [13,15]. Below the Néel temperature $T_N = 153$ K, the antiferromagnetic (AFM) G-type ground state is stabilized on the diluted magnetic lattice of Fe^{3+} ions [14,16]. At low temperature $T_g = 10.6$ K, a spin cluster glass state coexisting with the G-type AFM one is formed [10,11].

The classical oxide multiferroic materials demonstrate a general trend towards a suppression of ferroelectricity and/or magnetoelectric coupling under pressure, as experimentally found for $BiFeO_3$ and hexagonal $RMnO_3$ [17–19] This behavior is in-line with a tendency for a suppression of ferroelectricity in displacement-type ferroelectrics under pressure [20].

In comparison with conventional multiferroics, the pressure behavior of relaxor multiferroic materials remains poorly explored. The relaxor multiferoric $PbFe_{0.5}Nb_{0.5}O_3$ is a suitable model system to gain insight into high-pressure effects on structural, magnetic, and multiferroic properties of such systems. A study of the dielectric properties of $PbFe_{0.5}Nb_{0.5}O_3$ at moderate pressures up to 0.6 GPa revealed a reduction of the ferroelectric transition temperature, indicating instability of the ambient pressure rhombohedral polar phase [21]. In order to study in detail the high-pressure effects on the crystal structure and magnetic and vibrational properties of relaxor multiferroic $PbFe_{0.5}Nb_{0.5}O_3$, we have performed powder x-ray and neutron diffraction, as well as Raman spectroscopy experiments in the 0–30 GPa pressure range.

II. EXPERIMENTAL

The $PbFe_{0.5}Nb_{0.5}O_3$ sample was prepared by standard two-stage ceramic technology using a mixture of chemically pure powders PbO, Fe_2O_3, and Nb_2O_5, taken in stoichiometric ratio. A synthesis was performed at a temperature of 1000 °C for 2.5 h in the air environment and sintering at 1150 °C for 3.5 h, with the subsequent cooling in a mode of the switched off furnace [22].

Angle-dispersive x-ray powder diffraction patterns at high pressures up to 30 GPa and ambient temperature were measured at the Extreme Conditions Beamline [23] P02.2 at the third-generation synchrotron radiation source PETRA III located at the Deutsches Elektronen Synchrotron (DESY), Hamburg, Germany. The diffraction images were collected with the wavelength $\lambda = 0.29118$ Å on the amorphous silicon flat panel detector bonded to a ScI scintillator (XRD 1621) from Perkin Elmer and located at a distance of 402.33 mm from the sample. The two-dimensional x-ray diffraction (XRD) images were converted to one-dimensional diffraction patterns using the FIT2D program [24].

Raman spectra at ambient temperature and pressures up to 30 GPa were collected using a LabRam spectrometer (NeHe excitation laser) with a wavelength of 632.8 nm, 1800 grating, confocal hole of 1100 μm, and a 50× objective. The BX90-type diamond anvil cell [25] was used for the x-ray diffraction and Raman experiments. The sample was loaded into the hole of the 120-μm diameter made in the Re gasket intended to be ~30-μm thickness. The diamonds with culets of 250 μm were used. Neon gas loaded under pressure of ~0.15 GPa was used as a pressure-transmitting medium. The pressure was determined by the ruby fluorescence technique [26].

Neutron powder diffraction measurements at high pressures up to 6.4 GPa were performed at selected temperatures in the range of 10–290 K with the DN-12 spectrometer [27] at the IBR-2 high-flux pulsed reactor [Frank Laboratory of Neutron Physics, Joint Institute for Nuclear Research (JINR), Dubna, Russia]. The sample with a volume of ~2 mm^3 was loaded into the sapphire anvil high-pressure cell [28]. Several tiny ruby chips were placed at different points of the sample surface, and the pressure was determined by a standard ruby fluorescence technique. Measurements of the pressure distribution on the sample yield typical pressure inhomogeneities of ±15%. Diffraction patterns were collected at scattering angle 90°, with the resolution $\Delta d/d = 0.015$. Experimental data of the x-ray and neutron powder diffraction experiments were analyzed by the Rietveld method using the FULLPROF [29] and MRIA [30] programs.

III. RESULTS AND DISCUSSION

A. X-ray diffraction

X-ray diffraction patterns of $PbFe_{0.5}Nb_{0.5}O_3$ at selected pressures and ambient temperature are shown in Fig. 1. For the description of the experimental data at moderate pressures, the rhombohedral *R*3*m* and monoclinic *Cm* models were tested. The analysis by the Rietveld method has shown that the rhombohedral structural model is in better agreement with the experimental data than the monoclinic one; thus, we have

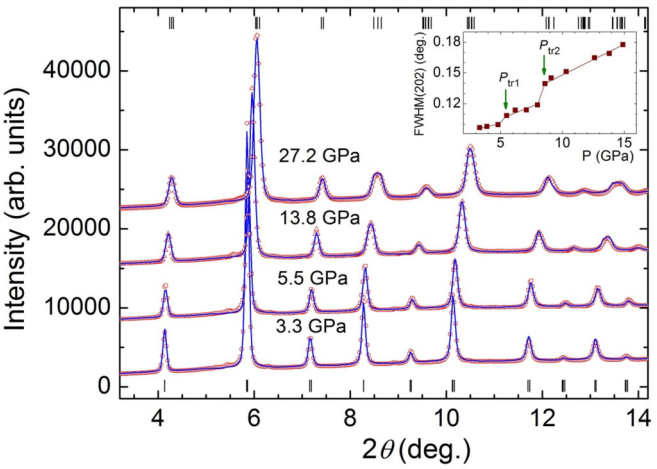

FIG. 1. (Color online) X-ray diffraction patterns of $PbFe_{0.5}Nb_{0.5}O_3$ measured at selected pressures and ambient temperature and refined by the Rietveld method. Experimental points and calculated profiles are shown. Tick marks at the bottom and top represent the calculated positions of diffraction peaks for the *R*3*m* rhombohedral phase (at $P = 3.3$ GPa) and *Pm* monoclinic phase (at $P = 27.2$ GPa), respectively. Inset: pressure dependence of the full width at half maximum of the diffraction peak, corresponding to (202) reflection of the rhombohedral phase.

chosen the rhombohedral model for further evaluations. The corresponding weighted *R*-factor values, obtained at $P = 3.3$ GPa, are $R_{wp} = 3.98\%$ for the *R*3*m* model and 4.12% for the *Cm* model. One should note that the average lattice symmetry of disordered compounds, such as $PbFe_{0.5}Nb_{0.5}O_3$, depends on the features of the local atomic order, which may be distinctive for the samples synthesized by different procedures. The difference between *R* factors obtained for the *R*3*m* and *Cm* models is relatively small, and the present data could not exclude unambiguously the *Cm* model. However, the *R*3*m* symmetry of the ambient pressure crystal structure of $PbFe_{0.5}Nb_{0.5}O_3$ is also supported by the analysis of the experimental behavior of the quadratic paramagnetoelectric effect [10].

At pressures above 5 GPa, an additional broadening of the diffraction peak located at $2\theta = 8.3°$, corresponding to the single (202) reflection in the initial rhombohedral *R*3*m* phase (indexes are given in hexagonal setting), was evidenced (Fig. 1, inset). This implies the appearance of a structural phase transformation, which leads to a lowering of the lattice symmetry. A splitting of the (202) peak into two components is expected for the tetragonal structure of *P*4*mm* symmetry, found in $PbFe_{0.5}Nb_{0.5}O_3$ at elevated temperatures or for the monoclinic structure with *Cm* symmetry previously discussed. Both models were tested in the diffraction data refinements by the Rietveld method, and better fitting quality was achieved for the monoclinic *Cm* model. The corresponding weighted *R*-factor values, obtained at $P = 5.5$ GPa, are $R_{wp} = 3.24\%$ for the *P*4*mm* model and 3.01% for the *Cm* model.

At pressures above 8.5 GPa, a drastic broadening of the diffraction peaks located at $2\theta = 8.4$, 10.3, and 13.4° was detected (Fig. 1), indicating the appearance of one more structural transformation, causing further lowering of

TABLE I. Structural parameters of the rhombohedral and monoclinic phases of $PbFe_{0.5}Nb_{0.5}O_3$ at selected pressures and ambient temperature. The R_p and R_{wp} factors values are also given.

P (GPa)	3.3	5.5	13.8	27.2
Symmetry	$R3m$	Cm	Pm	Pm
Lattice parameters				
a (Å)	5.6775(8)	5.6092(8)	3.9093(6)	3.8451(7)
b (Å)	—	5.6243(8)	3.9353(6)	3.8826(8)
c (Å)	6.9536(8)	3.9574(6)	3.8875(6)	3.8121(7)
β (deg)	—	89.66(7)	89.67(7)	89.54(9)
Atomic coordinates				
Pb: x	0	0	0	0
y	0	0	0	0
z	0	0	0	0
Fe/Nb: x	0	0.469(4)	0.490(4)	0.480(5)
y	0	0	0.5	0.5
z	0.483(3)	0.485(4)	0.492(4)	0.500(5)
O1: x	0.184(5)	0.489(8)	0.534(9)	0.582(9)
y	−0.184(5)	0	0	0
z	0.328(9)	0.039(8)	0.520(9)	0.490(9)
O2: x	—	0.229(8)	0.512(9)	0.524(9)
y	—	0.202(8)	0.5	0.5
z	—	0.491(8)	0.068(9)	0.079(9)
O3: x	—	—	0.028(9)	0.067(5)
y	—	—	0.5	0.5
z	—	—	0.524(9)	0.536(9)
R_p (%)	3.30	2.53	2.12	2.26
R_{wp} (%)	3.98	3.01	2.73	2.87

the lattice symmetry. The consideration of the pressure behavior of the diffraction peak located at $2\theta = 8.4°$ has shown that it splits into three components with comparable intensity. Subsequent analysis by the Rietveld method has shown that the structural monoclinic model of Pm symmetry provides good description of the experimental data ($R_{wp} = 2.73\%$ for $P = 13.8$ GPa). The monoclinic Pm phase was observed previously at ambient conditions in relevant Pb-based systems $(PbSc_{1/2}Nb_{1/2}O_3)_{1-x}$-$(PbTiO_3)_x$, $(PbMg_{1/3}Nb_{2/3}O_3)_{1-x}$-$(PbTiO_3)_x$, and $(PbZn_{1/3}Nb_{2/3}O_3)_{1-x}$-$(PbTiO_3)_x$ [31,32].

The structural parameters of the initial rhombohedral and two pressure-induced monoclinic phases of $PbFe_{0.5}Nb_{0.5}O_3$ are presented in Table I. The pressure dependencies of lattice parameters and unit cell volume of the observed phases of $PbFe_{0.5}Nb_{0.5}O_3$ are shown in Fig. 2. The lattice compression is anisotropic with the c axis being the most compressible in the rhombohedral and monoclinic phases. In both Cm and Pm high-pressure phases, the monoclinic angle decreases slightly upon compression, and it exhibits a jump at the transition pressure (Fig. 2). The volume compressibility data (Fig. 2) were fitted by the third-order Birch-Murnaghan equation of state [33]:

$$P = \tfrac{3}{2}B_0(x^{-7/3} - x^{-5/3})\left[1 + \tfrac{3}{4}(B' - 4)(x^{-2/3} - 1)\right],$$

where $x = V/V_0$ is the relative volume change, V_0 is the unit cell volume at ambient pressure, and B_0, B' are the bulk modulus ($B_0 = -V(dP/dV)_T$) and its pressure derivative ($B' = (dB_0/dP)_T$). The fitted values $B_0 = 135(5)$ GPa, $B' = 4.0(5)$, and $V_0 = 194.1(4)$ Å^3 for the rhombohedral $R3m$ phase, $B_0 = 140(5)$ GPa, $B' = 4.0(5)$, and $V_0 = 129.4(3)$ Å^3 for the monoclinic Cm phase, and $B_0 = 195(5)$ GPa, $B' = 4.0(5)$, $V_0 = 63.6(1)$ Å^3 for the monoclinic Pm phase were obtained, respectively. The bulk modulus values of the $R3m$ and Cm phases of $PbFe_{0.5}Nb_{0.5}O_3$ are noticeably larger in comparison with those for the cubic $Fm\bar{3}m$ compositionally ordered phase of $PbSc_{0.5}Ta_{0.5}O_3$ ($B_0 \approx 110$ GPa), rhombohedral $R3c$ phase of $BiFeO_3$ ($B_0 = 99$ GPa) and moderate pressure tetragonal $P4mm$ phase of $PbTiO_3$ ($B_0 = 100$ GPa) [34,17,35]. The B_0 value for the monoclinic Pm phase is close to one obtained for the cubic perovskite $Pm\bar{3}m$ high-pressure phase of $PbTiO_3$ ($B_0 = 195$ GPa) [35].

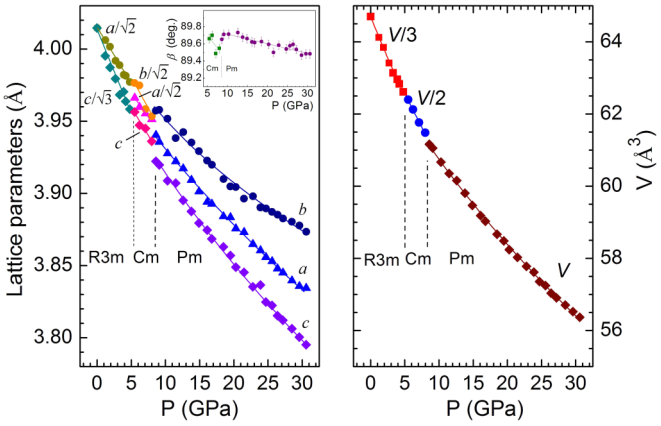

FIG. 2. (Color online) Lattice parameters (left), monoclinic angle (left, inset), and unit cell volume (right) as functions of pressure in the rhombohedral and monoclinic phases of $PbFe_{0.5}Nb_{0.5}O_3$.

B. Neutron diffraction

Neutron diffraction patterns of $PbFe_{0.5}Nb_{0.5}O_3$, measured at selected pressures and temperatures, are shown in Fig. 3. The observed broadening of the diffraction peaks upon

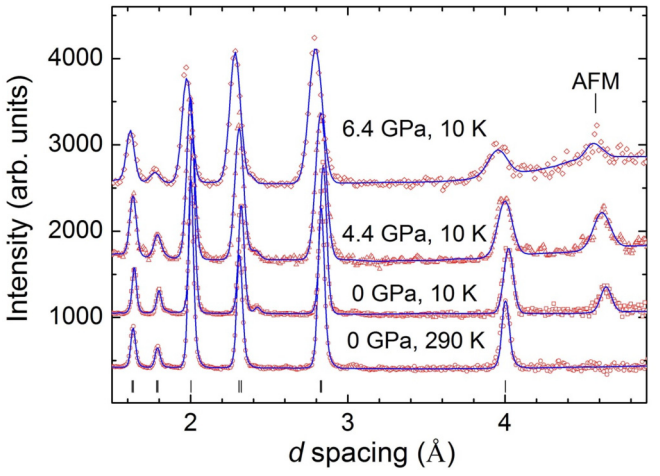

FIG. 3. (Color online) Neutron diffraction patterns of $PbFe_{0.5}Nb_{0.5}O_3$, measured at selected pressures and temperatures and processed by the Rietveld method. The experimental points and calculated profiles are shown. Tick marks below represent calculated positions of the nuclear peaks of the rhombohedral phase at ambient conditions. The most intense magnetic peak is marked as AFM.

compression reflects the contribution from the pressure gradients in the sapphire anvil high-pressure cell. At ambient pressure below $T_N = 155$ K, an appearance of the intense magnetic peak (1 0 1/2) at $d = 4.63$ Å was observed (indices are given with respect to the rhombohedral unit cell of the atomic structure in a hexagonal setting), characteristic for the G-type AFM order onset. The calculated value of the Fe-ordered magnetic moment, $\mu_{Fe} = 2.6(1)\ \mu_B$ at $T = 10$ K, is consistent with previous ambient pressure studies [14]. It is significantly lower in comparison with the expected spin-only value 5 μ_B for Fe $^{3+}$ ($3d^5$) ion and that 5.93 μ_B experimentally found from paramagnetic susceptibility measurements [36]. This observation is consistent with the cluster approach for a description of the magnetic ground state of $PbFe_{0.5}Nb_{0.5}O_3$ [10]. The ordered magnetic moment is associated with the percolating exchange-coupled infinite Fe^{3+} cluster, while its reduction from the spin-only value is caused by the presence of the finite Fe^{3+} clusters and isolated Fe^{3+} ions. The latter ones contribute to the spin-glass state observed at temperatures below $T_g = 10.6$ K [10,11]. In the recent study of $PbFe_{0.5}Nb_{0.5}O_3$ by means of Mössbauer spectroscopy and neutron diffraction, it was proposed that all Fe^{3+} spins contribute to the AFM ground state, and the magnetic ground state is a microscopic coexistence of the AFM and spin-glass orders [37]. The features of the magnetic ground state of the $PbFe_{0.5}Nb_{0.5}O_3$ are controlled by a spatial uniformity of the chemical disorder of magnetic Fe^{3+} and nonmagnetic Nb^{5+} ions over the sample volume and depend on the sample synthesis procedure. For the ideally uniform distribution of Fe^{3+} and Nb^{5+} ions in the sample volume, the homogeneous magnetic ground state [37] is expected, while for the samples containing rich Fe^{3+} and Nb^{5+} volume regions, the cluster model of the ground state [10] is more appropriate, as for the sample studied in this paper.

The temperature dependencies of the Fe-ordered magnetic moments at selected pressures are shown in Fig. 4. In the pressure range achieved in neutron diffraction experiments, 0–6.4 GPa, nearly linear increase of the Néel temperature up to 167 K with a pressure coefficient $(1/T_N)dT_N/dP = 0.012$ GPa^{-1} is observed. This value is comparable with relevant coefficients for ferrites $NdFeO_3$ and $LuFeO_3$, 0.016 and 0.014 GPa^{-1}, respectively [38]. The Fe ordered magnetic moment value at the lowest temperature achieved in experiments, $T = 10$ K, remains about the same upon compression.

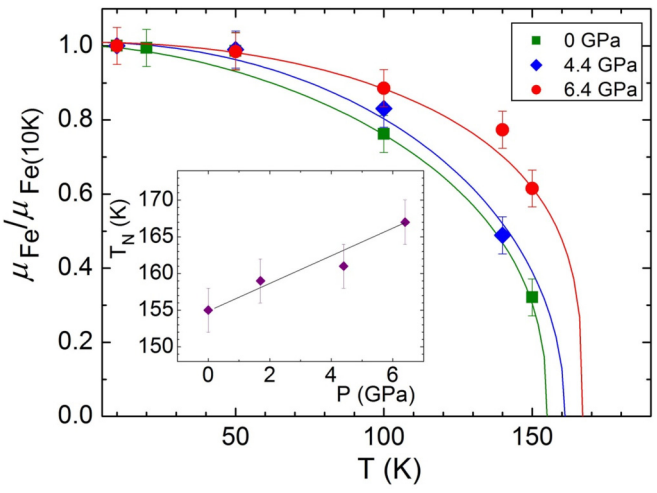

FIG. 4. (Color online) Temperature dependencies of the ordered Fe magnetic moment at selected pressures, normalized to the values obtained at $T = 10$ K. The solid lines represent interpolations by functions $\mu = \mu_0(1\text{-}(T/T_N)^\alpha)^\beta$. Inset: pressure dependence of the Néel temperature and its linear interpolation.

C. Raman spectroscopy

The Raman spectra of $PbFe_{0.5}Nb_{0.5}O_3$ measured at selected pressures and ambient temperature, are shown in Fig. 5. At ambient pressure, ten lines at 203.1, 255.4, 298.1, 320.3, 429.2, 473.6, 558.0, 711.5, 791.4, and 849.3 cm^{-1} are detected. For the ideal rhombohedral $R3m$ symmetry, the group theory predicts seven Raman active modes, $\Gamma_{Ram} = 3A_1 + 4E$ [39]. However, cationic disorder leads to a local symmetry breaking, and it is well established that Raman spectra of disordered relaxor materials contain more lines than expected for the ideal symmetry of the crystal structure. As a good approximation, the $Fm\bar{3}m$ symmetry, corresponding to the ideal periodic alternation of the two types of cations at B-position in the simplified cubic perovskite ABO_3 lattice in three dimensions is commonly used for the description of the Raman spectra of such complex materials [39]. For this symmetry, the group theory predicts $A_{1g} + E_g + F_{1g} + 4F_{1u} + 2F_{2g} + F_{2u}$ optical phonon modes at the Brillouin zone center. Among these modes, four $A_{1g} + E_g + 2F_{2g}$ phonons are purely Raman active, and the rest become visible in Raman spectra due to local structural distortions with respect to the ideal lattice. The tentative assignment of the observed modes, made according to previous studies of $PbFe_{0.5}Nb_{0.5}O_3$ at ambient pressure [40,41], and also Pb-based relaxor oxides [34,39,42] are presented in Table II. The modes located in the region 700–850 cm^{-1} correspond to stretching vibrations of oxygen

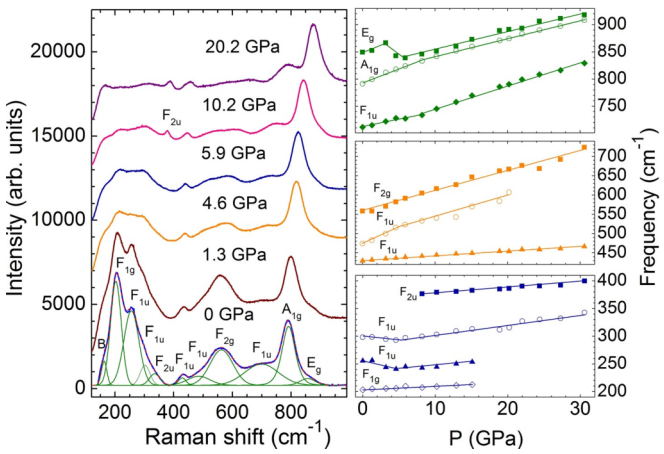

FIG. 5. (Color online) Raman spectra of $PbFe_{0.5}Nb_{0.5}O_3$ at selected pressures. For ambient pressure spectrum, the fitting result by a set of pseudo-Voigt functions is also shown (left). The modes assignment according to the Table II is given. The peak marked as "B" is added for a description of the spectrometer cutoff contribution to the Raman spectra at small Raman shift values. Pressure dependencies of the selected vibrational modes frequencies (right). The error bars are within the symbol sizes.

TABLE II. Assignment and pressure coefficients ($1/v_{i0}dv_i/dP$) of Raman modes in the rhombohedral and monoclinic phases of $PbFe_{0.5}Nb_{0.5}O_3$. (sym.: symmetric and asym.: asymmetric.)

Mode (cm^{-1})	Assignment	Pressure coefficient (GPa^{-1})		
		*R*3*m* phase	*Cm* phase	*Pm* phase
849.3 (0 GPa)	E_g sym. Fe/Nb-O stretching	0.006	− 0.004	—
791.4 (0 GPa)	A_{1g} sym. Fe/Nb-O stretching	0.007	0.007	0.004
711.5 (0 GPa)	F_{1u} asym. Fe/Nb-O stretching	0.005	0.005	0.006
558.0 (0 GPa)	F_{2g} sym. O-Fe/Nb-O bending	0.010	0.010	0.009
473.6 (0 GPa)	F_{1u} asym. O-Fe/Nb-O bending	0.018	0.018	0.009
429.2 (0 GPa)	F_{1u} asym. O-Fe/Nb-O bending	0.003	0.003	0.002
376.4 (8.2 GPa)	F_{2u} Pb-O bond stretching	—	—	0.002
320.3 (0 GPa)	F_{2u} Pb-O bond stetching	0.017	0.017	—
298.1 (0 GPa)	F_{1u} localized	− 0.004	0.006	0.006
255.4 (0 GPa)	F_{1u} localized	− 0.012	0.005	0.005
203.1 (0 GPa)	F_{1g} octahedral rotation	0.003	0.003	0.003

octahedra around Fe/Nb atoms of A_{1g} (791.4 cm^{-1}), E_g (849.3 cm^{-1}), and F_{1u} (711.5 cm^{-1}) symmetry. The region of 400–530 cm^{-1} involves the bending O-Fe/Nb-O vibrations of F_{2g} (558.0 cm^{-1}) and F_{1u} (473.6, 429.2 cm^{-1}) symmetry. The modes at the region of 200–400 cm^{-1} are related to Pb-O bond stretching vibrations of F_{2u} symmetry (320.3 cm^{-1}), Fe/Nb-cation localized mode of F_{1u} symmetry (255.4, 298.1 cm^{-1}), and the rotational mode of Fe/Nb-O6 octahedra of F_{1g} symmetry (203.1 cm^{-1}).

Upon compression in the rhombohedral *R*3*m* phase, a softening of the Fe/Nb localized modes occurs (Fig. 5). The presence of these modes in the Raman spectra is activated by cation dynamical off-centered shifts, and the observed behavior implies their instability with respect to the pressure-induced structural rearrangement in the vicinity of the phase transition. The frequencies of the rest of the observed phonon modes increase under pressure with the larger pressure coefficients for the Pb-O stretching and O-Fe/Nb-O bending modes and smaller ones for the Fe/Nb-O_6 octahedra stretching modes (Table II). In the region of the *R*3*m*-*Cm* structural phase transition at $P \sim 5$ GPa, a rapid softening of the E_g stretching mode and a change in the slope of pressure dependencies of the localized and bending F_{1u} modes occur (Fig. 5). In the *Cm* phase, the behavior of all the observed modes, including the Fe/Nb localized and stretching ones, restores to normal character with positive pressure coefficients (Fig. 5; Table II). The observed anomalies in the pressure behavior of the Fe/Nb localized, stretching, and bending modes point out the lattice symmetry change at the structural phase transition and support the *R*3*m*-*Cm* model of the structural phase transition. A possible alternative scenario of the structural modifications within the same *Cm* symmetry under pressure is not consistent with the observations previously mentioned.

In the region of the *Cm*-*Pm* transition at $P \sim 8.5$ GPa, an appearance of a new Raman line at 376.4 cm^{-1} and a slope change of pressure dependencies of the stretching A_{1g}, F_{1u} modes have been detected (Fig. 5). The origin of the extra line can be related to a further splitting of the Pb-O bond stretching mode of F_{2u} symmetry, caused by symmetry lowering. Its presence implies a persistence of the ferroic off-centered Pb shifts in the *Pm* monoclinic high-pressure phase of $PbFe_{0.5}Nb_{0.5}O_3$ [34,39].

Under pressure, a decrease of the intensity and broadening of the Fe/Nb localized modes in the 250–300 cm^{-1} region was observed (Fig. 5). This observation implies a reduction of the cationic off-centered ferroic shifts under pressure [42,43]. Indeed, the values of the Fe/Nb shifts from the centrosymmetric positions evaluated from structural data (Table I) are $\delta_{Fe/Nb} \approx 0.06$–$0.07$ Å in the *Pm* phase at pressures 13.8–27.2 GPa, which are about twice smaller in comparison with those in the rhombohedral *R*3*m* phase, $\delta_{Fe/Nb} \approx 0.12$ Å ($P = 3.3$ GPa). As a result, for the *Pm* phase, the pressure dependencies of the Fe/Nb localized modes and closely located weak Pb-O stretching mode were obtained in the limited pressure range only. In all the observed phases of $PbFe_{0.5}Nb_{0.5}O_3$, the pressure coefficients of the O-Fe/Nb-O bending modes are larger in comparison with those of the stretching modes of Fe/Nb-O_6 oxygen octahedra (Table II). This indicates that the compressibility of the Pb-O bonds provides a more significant contribution to lattice contraction in comparison with less compressible Fe/Nb-O bonds.

Let us compare the effects of high external pressure and chemical pressure on relaxor ferroics with perovskite structure. The observed sequence of the pressure-induced structural phase transitions *R*3*m*-*Cm*-*Pm* in $PbFe_{0.5}Nb_{0.5}O_3$ is the same as found upon chemical substitution in the related system $(PbSc_{0.5}Nb_{0.5}O_3)_{1-x}$-$(PbTiO_3)_x$ for $0 < x < 0.55$, leading to lattice volume contraction [31]. In the latter case, the local chemical and polar inhomogeneities are also drastically modified due to the difference of the valence state of Ti^{4+} and Sc^{3+}/Nb^{5+} ions. The qualitative similarity of external pressure and chemical substitution response clearly demonstrates an important role of lattice degrees of freedom in the formation of the physical properties of complex ferroic relaxor materials.

All the observed pressure-induced rhombohedral and monoclinic phases of relaxor $PbFe_{0.5}Nb_{0.5}O_3$ are polar and allow ferroelectricity. The stability of the magnetic order with increasing T_N value implies a multiferroic character of high-pressure phases. In contrast, the general trend of the pressure behavior of classical multiferroics is a suppression of ferroelectricity and/or magnetoelectric coupling [17–19]. In addition, the displacement-type perovskite ferroelectrics ABO_3 generally exhibit a suppression of the ferroelectricity and a stabilization of the cubic perovskite nonpolar $Pm\bar{3}m$

phase [20]. Moreover, the character of pressure-induced structural phase transitions in chemically disordered multiferroic $PbFe_{0.5}Nb_{0.5}O_3$ is distinctive from that observed in the relevant nonmagnetic relaxor ferroelectric $PbSc_{0.5}Ta_{0.5}O_3$ and $PbSc_{0.5}Nb_{0.5}O_3$ with a *B*-site cationic compositional order and initial cubic crystal structure of $Fm\bar{3}m$ symmetry. In these compounds, two structural transformations to nonpolar rhombohedral and monoclinic phases were detected upon compression [34,44].

One should also note that in a few exceptional cases a re-entrant ferroelectric behavior were recently experimentally found at very high pressures ~45 GPa. In $PbTiO_3$, a sequence of structural phase transformations $Pm\bar{3}m$-$I4/mcm$-$I4cm$ occurs under pressure [45]. In relaxor $PbZn_{1/3}Nb_{2/3}O_3$, structural phase transformations $R3m$-$R\bar{3}c$-$C2/c$-Cc were observed upon compression [46].

IV. CONCLUSIONS

Our results demonstrate the application of high pressure leads to successive $R3m$-Cm-Pm structural phase transitions in relaxor multiferroic $PbFe_{0.5}Nb_{0.5}O_3$, accompanied by anomalies in pressure behavior of stretching, bending, and Fe/Nb localized vibrational modes. The polar symmetry and a stability of the *G*-type AFM magnetic order with a positive pressure coefficient of the Néel temperature assumes a possible multiferroic character of the pressure-induced phases. In order to explore the features of the magnetoelectric coupling in high-pressure phases of $PbFe_{0.5}Nb_{0.5}O_3$, further experimental studies are necessary.

The observation of the polar phases with assumed multiferroic properties in relaxor $PbFe_{0.5}Nb_{0.5}O_3$ is in drastic contrast with a general trend towards a suppression of ferroelectricity and/or magnetoelectric coupling under pressure, observed in the most of the conventional oxide multiferroics.

The similarity between sequence of the phase transitions induced by high external pressure in $PbFe_{0.5}Nb_{0.5}O_3$ and volume reduction by chemical substitution (chemical pressure) in relevant $(PbSc_{0.5}Nb_{0.5}O_3)_{1-x}$-$(PbTiO_3)_x$ system demonstrates that not only compositional disorder effects but also lattice degrees of freedom themselves play an important role in the formation of physical properties of relaxor ferroic materials.

ACKNOWLEDGMENTS

The work has been supported by the Russian Foundation for Basic Research (RFBR) Grant No. 12-02-00794-a. The authors acknowledge useful discussions with Dr. A. V. Belushkin (JINR, Dubna, Russia). Portions of this research were carried out at the light source PETRA III at DESY, a member of the Helmholtz Association. Financial support from the Bundesministerium fur Bildung und Forschung (BMBF), Germany (Projects No. 05K10RFA and No. 05K13RF1) is gratefully acknowledged.

[1] G. A. Smolenskii and I. E. Chupis, Sov. Phys. Usp. **25**, 475 (1982).
[2] M. Fiebig, J. Phys. D **38**, R123 (2005).
[3] T. Kimura, T. Goto, H. Shintani, K. Ishizaka, T. Arima, and Y. Tokura, Nature (London) **426**, 55 (2003).
[4] S.-W. Cheong and M. Mostovoy, Nat. Mater. **6**, 13 (2007).
[5] M. Kenzelmann, G. Lawes, A. B. Harris, G. Gasparovic, C. Broholm, A. P. Ramirez, G. A. Jorge, M. Jaime, S. Park, Q. Huang, A. Ya. Shapiro, and L. A. Demianets, Phys. Rev. Lett. **98**, 267205 (2007).
[6] A. Levstik, C. Filipic, and J. Holc, J. Appl. Phys. **103**, 066106 (2008).
[7] E. I. Sitalo, I. P. Raevski, A. G. Lutokhin, S. P. Kubrin, S. I. Raevskaya, Yu. N. Zakharov, M. A. Malitskaya, A. V. Blazhevich, and I. N. Zakharchenko, Ferroelectrics **419**, 76 (2011).
[8] Yu. N. Zakharov, S. I. Raevskaya, A. G. Lutokhin, V. V. Titov, I. P. Raevski, V. G. Smotrakov, V. V. Eremkin, A. S. Emelyanov, and A. A. Pavelko, Ferroelectrics **399**, 20 (2010).
[9] S. A. Gridnev and A. A. Kamynin, Phys. Solid State **54**, 1018 (2012).
[10] W. Kleemann, V. V. Shvartsman, P. Borisov, and A. Kania, Phys. Rev. Lett. **105**, 257202 (2010).
[11] G. M. Rotaru, B. Roessli, A. Amato, S. N. Gvasaliya, C. Mudry, S. G. Lushnikov, and T. A. Shaplygina, Phys. Rev. B **79**, 184430 (2009).
[12] G. A. Smoilenskii, A. I. Agranovskaia, S. N. Popov, and V. A. Isupov, Sov. Phys. Tech. Phys. **3**, 1981 (1958).
[13] V. Bonny, M. Bonin, P. Sciau, K. J. Schenk, and G. Chapuis, Solid State Commun. **102**, 347 (1997).
[14] S. A. Ivanov, R. Tellgren, H. Rundlof, N. W. Thomas, and S. Ananta, J. Phys.: Condens. Matter **12**, 2393 (2000).
[15] N. Lampis, P. Sciau, and A. G. Lehmann, J. Phys.: Condens. Matter **11**, 3489 (1999).
[16] V. A. Bokov, I. E. Myl'nikova, and G. A. Smolensky, Sov. Phys. JETP **15**, 447 (1962).
[17] D. P. Kozlenko, A. A. Belik, A. V. Belushkin, E. V. Lukin, W. G. Marshall, B. N. Savenko, and E. Takayama-Muromachi, Phys. Rev. B **84**, 094108 (2011).
[18] D. P. Kozlenko, I. Mirebeau, J.-G. Park, I. N. Goncharenko, S. Lee, J. Park, and B. N. Savenko, Phys. Rev. B **78**, 054401 (2008).
[19] D. P. Kozlenko, S. E. Kichanov, S. Lee, J.-G. Park, and B. N. Savenko, J. Phys.: Condens. Matter **19**, 156228 (2007).
[20] G. A. Samara, T. Sakudo, and K. Yoshimitsu, Phys. Rev. Lett. **35**, 1767 (1975).
[21] N. Yasuda and Y. Ueda, J. Phys.: Condens. Matter **1**, 5179 (1989).
[22] S. A. Gridnev and A. A. Kamynin, Bull. Russ. Acad. Sci. Phys. **75**, 1371 (2011).
[23] H.-P. Liermann, W. Morgenroth, A. Ehnes, A. Berghäuser, B. Winkler, H. Franz, and E. Weckert, J. Phys. Conf. Ser. **215**, 012029 (2010).
[24] A. P. Hammersley, S. O. Svensson, M. Hanfland, A. N. Fitch, and D. Hausermann, High Press. Res. **14**, 235 (1996).
[25] N. A. Dubrovinskaia and L. S. Dubrovinsky, Rev. Sci. Instrum. **74**, 3433 (2003).
[26] H. K. Mao, P. M. Bell, J. W. Shaner, and D. J. Steinberg, J. Appl. Phys. **49**, 3276 (1978).

[27] V. L. Aksenov, A. M. Balagurov, V. P. Glazkov, D. P. Kozlenko, I. V. Naumov, B. N. Savenko, D. V. Sheptyakov, V. A. Somenkov, A. P. Bulkin, V. A. Kudryashev, and V. A. Trounov, Physica B **265**, 258 (1999).
[28] V. P. Glazkov and I. N. Goncharenko, Fiz. I Technika Vysokih Davlenij **1**, 56 (1991) (in Russian).
[29] J. Rodríguez-Carvajal, Physica B **192**, 55 (1993).
[30] V. B. Zlokazov and V. V. Chernyshev, J. Appl. Cryst. **25**, 447 (1992).
[31] R. Haumont, P. Gemeiner, B. Dkhil, J. M. Kiat, and A. Bulou, Phys. Rev. B **73**, 104106 (2006).
[32] J. M. Kiat, Y. Uesu, B. Dkhil, M. Matsuda, C. Malibert, and G. Calvarin, Phys. Rev. B **65**, 064106 (2002).
[33] F. J. Birch, J. Geophys. Res. **91**, 4949 (1986).
[34] B. Mihailova, R. J. Angel, A. M. Welsch, J. Zhao, J. Engel, C. Paulmann, M. Gospodinov, H. Ahsbahs, R. Stosch, B. Güttler, and U. Bismayer, Phys. Rev. Lett. **101**, 017602 (2008).
[35] A. Sani, M. Hanfland, and D. Levy, J. Phys.: Condens. Matter **14**, 10601 (2002).
[36] A. Maryanowska and J. Pietrzak, Ferroelectrics **162**, 81 (1994).
[37] S. Chillal, M. Thede, F. J. Litterst, S. N. Gvasaliya, T. A. Shaplygina, S. G. Lushnikov, and A. Zheludev, Phys Rev. B **87**, 220403 (2013).
[38] A. G. Gavriliuk, G. N. Stepanov, I. S. Lyubutin, A. S. Stepin, I. A. Trojan, and V. A. Sidorov, Hyperfine Interact. **126**, 305 (2000).
[39] B. Mihailova, U. Bismayer, B. Güttler, M. Gospodinov, and L. Konstantinov, J. Phys.: Condens. Matter **14**, 1091 (2002).
[40] A. F. Garsía-Flores, D. A. Tenne, Y. J. Choi, W. J. Ren, X. X. Xi, and S. W. Cheong, J. Phys.: Condens. Matter **23**, 015401 (2011).
[41] M. Correa, A. Kumar, S. Priya, R. S. Katiyar, and J. F. Scott, Phys. Rev. B **83**, 014302 (2011).
[42] B. Mihailova, B. Maier, C. Paulmann, T. Malcherek, J. Ihringer, M. Gospodinov, R. Stosch, B. Güttler, and U. Bismayer, Phys. Rev. B **77**, 174106 (2008).
[43] A.-M. Welsch, B. Mihailova, M. Gospodinov, R. Stosch, B. Güttler, and U. Bismayer, J. Phys.: Condens. Matter **21**, 235901 (2009).
[44] B. J. Maier, N. Waeselmann, B. Mihailova, R. J. Angel, C. Ederer, C. Paulmann, M. Gospodinov, A. Friedrich, and U. Bismayer, Phys. Rev. B **84**, 174104 (2011).
[45] P.-E. Janolin, P. Bouvier, J. Kreisel, P. A. Thomas, I. A. Kornev, L. Bellaiche, W. Crichton, M. Hanfland, and B. Dkhil, Phys. Rev. Lett. **101**, 237601 (2008).
[46] P.-E. Janolin, B. Dkhil, P. Bouvier, J. Kreisel, and P. A. Thomas, Phys. Rev. B **73**, 094128 (2006).